JOURNAL OF GEOPHYSICAL RESEARCH, VOL. 115, B04312, doi:10.1029/2009JB006420, 2010

On the absence of an ultralow-velocity zone in the North Pacific

Sebastian Rost,[1] Edward J. Garnero,[2] Michael S. Thorne,[3] and Alexander R. Hutko[4,5]

Received 2 March 2009; revised 18 October 2009; accepted 25 November 2009; published 15 April 2010.

[1] Using an unusually large earthquake near the big island of Hawaii, we study the core mantle boundary (CMB) beneath the north-northeastern Pacific between Hawaii and North America. A dense sampling of the CMB is achieved using the core-reflected phase *PcP* recorded at a large number of high-quality stations in North America, including networks in California, Oregon, Washington, and Alaska, as well as at EarthScope's USArray stations. We apply an adaptive stacking technique for optimal record alignment on specific phases (namely *P* and *PcP*) and subsequently stack seismograms to obtain summation traces possessing relatively high signal-to-noise ratios of *PcP* and *P*. Anomalous ultralow-velocity zone (ULVZ) layering at the CMB has been noted to exist in various parts of the Pacific beneath the lowermost mantle large low shear velocity province imaged by tomography. ULVZ structure produces anomalous *PcP* waveform variations in the form of precursors to *PcP*. These *PcP* data, however, lack precursory energy, indicating either that (1) ULVZ layering is lacking or (2) that a ULVZ is present and thinner than our detection threshold, i.e., less than a few kilometers thick. We use synthetic waveform modeling to establish the sensitivity and utility of investigating the time window ahead of *PcP* for precursors generated from fine-scale CMB layering. These results, combined with evidence for ULVZ structure in other parts of the Pacific, suggest that ULVZs are intermittent and possibly only detectable in regions where mantle currents collect ULVZ material, whether or not partially molten, presumably beneath (or near) upwellings or plumes.

Citation: Rost, S., E. J. Garnero, M. S. Thorne, and A. R. Hutko (2010), On the absence of an ultralow-velocity zone in the North Pacific, *J. Geophys. Res.*, *115*, B04312, doi:10.1029/2009JB006420.

1. Introduction

[2] Earth's core-mantle boundary (CMB) region continues to attract interest of scientists from all geodisciplines, as it likely plays a fundamentally important role in the evolution and dynamics of the planet's interior. The lowermost mantle near this boundary is host to many structural phenomena that demonstrate how this internal boundary is far from a simple contact zone between homogenous mantle rock and the fluid core [*Garnero*, 2000; *Lay and Garnero*, 2004; *Labrosse et al.*, 2007; *Duffy*, 2008]. Seismic velocity heterogeneity appears to increase in the lowermost few hundred kilometers of the mantle at a variety of scale lengths, from relatively long wavelength (e.g., 1000s of kilometers [*Masters et al.*, 2000]) to short scales (e.g., 10–100s of kilometers [*Garnero*, 2000]). The term D″ historically applies to this anomalous depth shell in general [*Bullen*, 1949] but in more recent decades commonly refers to a sharp discontinuous increase in seismic velocity about 200 to 300 km above the CMB [*Lay and Helmberger*, 1983; *Weber and Davis*, 1990; *Wysession*, 1996; *Wysession et al.*, 1998]. This region also shows evidence for seismic wave speed anisotropy [*Kendall and Silver*, 1996; *Lay et al.*, 1998] and scattering [*Bataille and Lund*, 1996; *Vidale and Hedlin*, 1998; *Hedlin and Shearer*, 2000]. The discontinuity (and possibly anisotropy) has been recently attributed to a phase transition in lower mantle magnesium perovskite [*Murakami et al.*, 2004; *Oganov and Ono*, 2004; *Hernlund et al.*, 2005; *Yamazaki et al.*, 2006]. These seismically detected structures point to the likely importance of the lowermost mantle in whole mantle processes and the evolution of the interior [*Garnero and McNamara*, 2008].

[3] In addition to these features, seismological evidence for thinner layering (of order 10s of kilometers and less) above and below the CMB exists [*Garnero et al.*, 1993, 1998; *Rost and Revenaugh*, 2001, 2003; *Thorne and Garnero*, 2004]. Thin ultralow-velocity zones (ULVZs) have been imaged in the lowermost 40 km of the mantle and are characterized by strong decreases in *P* wave and *S* wave velocities up to 10% and 30% relative to standard reference models, respectively [*Garnero and Helmberger*, 1995;

[1]Institute of Geophysics and Tectonics, School of Earth and Environment, University of Leeds, Leeds, UK.
[2]School of Earth and Space Exploration, Arizona State University, Tempe, Arizona, USA.
[3]Department of Geology and Geophysics, University of Utah, Salt Lake City, Utah, USA.
[4]Department of Earth Sciences, IGPP, University of California, Santa Cruz, California, USA.
[5]Now at U.S. Geological Survey, Golden, Colorado, USA.

0148-0227/10/2009JB006420

Williams and Garnero, 1996]. Recent studies also indicate a strong increase in ULVZ density of up to 10% in some locations [*Thorne and Garnero*, 2004; *Rost et al.*, 2005, 2006; *Garnero et al.*, 2007]. A variety of seismic probes permit investigation of ULVZ structure. Relatively large lateral scales (e.g., ≥ 100s of kilometers) can be pursued using phases with a portion of the wave path having *P* wave diffraction along the CMB, such as $SP_{diff}KS$ or $PKKP_{diff}$ [*Garnero and Helmberger*, 1995; *Thorne and Garnero*, 2004; *Rost and Garnero*, 2006]; smaller scales (few 10s of kilometers, laterally) can be studied using core reflected phases, such as *PcP*, *ScP*, and *ScS* [*Mori and Helmberger*, 1995; *Rost et al.*, 2005, 2006; *Avants et al.*, 2006; *Lay et al.*, 2006; *Idehara et al.*, 2007].

[4] Several mechanisms have been proposed as the origin of ULVZs. These include the existence of partial melt of the deepest mantle rock [*Williams and Garnero*, 1996; *Revenaugh and Meyer*, 1997; *Dubrovinsky et al.*, 2001; *Akins et al.*, 2004], the product of core and mantle material chemically reacting [*Knittle and Jeanloz*, 1991; *Song and Ahrens*, 1994], and mechanisms that produce iron enrichment in the lowermost mantle [*Dobson and Brodholt*, 2005; *Mao et al.*, 2006]. ULVZs have been proposed to be related to the roots of mantle plumes that give rise to hot spot volcanism [*Williams et al.*, 1998; *Rost et al.*, 2005], and argued to be most likely found in the hottest CMB regions, which may be near the margins of dense deep mantle thermochemical piles [*Garnero et al.*, 2007; *Garnero and McNamara*, 2008], owing to mantle upwellings preferentially extracting more core heat there. This is consistent with ULVZ possessing elevated density compared to the overlying mantle as geodynamical modeling shows that the densest material will be swept to these locations [*Rost et al.*, 2005, 2006; *Garnero et al.*, 2007; *McNamara et al.*, 2008].

[5] Distinguishing between different ULVZ hypotheses requires knowledge of the global distribution of ULVZs on Earth. However, only a limited number of regions have been probed to date, roughly half of the CMB's area. $SP_{diff}KS$ analyses account for roughly 40% of the globe being sampled [*Garnero et al.*, 1998; *Wen and Helmberger*, 1998; *Rondenay and Fischer*, 2003; *Thorne and Garnero*, 2004]; core-reflected data sample smaller individual areas in a variety of locations [*Reasoner and Revenaugh*, 2000; *Rost and Revenaugh*, 2003; *Persh and Vidale*, 2004; *Avants et al.*, 2006; *Idehara et al.*, 2007]. Thus, expanding the sampling coverage of the CMB is important. It is particularly relevant to consider locations of ULVZ positive detections with ULVZ nondetections, which might help to map lower mantle flow [*Garnero and McNamara*, 2008].

[6] The fact that ULVZs are not detected everywhere indicates that the ULVZ layer may not be global [*Vinnik et al.*, 1995; *Garnero et al.*, 1998; *Castle and van der Hilst*, 2000; *Reasoner and Revenaugh*, 2000; *Persh et al.*, 2001; *Thorne and Garnero*, 2004]. Since the CMB is assumed to be isothermal, a partial melt origin to ULVZ layering predicts a ubiquitous ULVZ if the base of the mantle is isochemical [*Lay et al.*, 2004]. Previous work noting ULVZ-free CMB zones may thus indicate ULVZ material of a different composition than the bulk of lower mantle and lateral chemical variations between ULVZ and non-ULVZ material. The vertical resolution of the seismic probes is limited. Nearly all past studies indicate fairly significant ULVZ resolution limitations in that ULVZ thickness must be at least 5–10 km in order to be seismically detected. This means that regions classified as non-ULVZ regions might contain ULVZ structure below this resolution. Indeed, ULVZs might exist everywhere but are generally too thin to be detected seismically. Therefore detected ULVZ regions might indicate only the thickest parts of a global ULVZ layer. Our ability to constrain a possible global ULVZ is hindered by the fact that only parts of the CMB have been probed for ULVZ structure so far. The primary reason why significant portions of the CMB have not been probed for ULVZ structure is the lack of suitable source-receiver geometries for the various ULVZ seismic probes.

[7] Here we study a new region just north of the large low shear velocity province (LLSVP) beneath the Pacific Ocean. Using core-reflected *PcP* waves and stacking methods to increase the signal-to-noise ratio of the reflected phases, we argue that a CMB region beneath the north-northeastern Pacific Ocean lacks any significant ULVZ structure and is possibly completely devoid of ULVZ structure. Stacked seismograms show *PcP* amplitudes clearly out of the background noise level, but no evidence for a *PcP* precursor that would indicate ULVZ existence. Using these new seismic results from this previously unprobed region of the CMB together with results from high-resolution convection simulations, we speculate that thicker (and hence detectable) ULVZs are most likely to be found near the margins between LLSVPs and the surrounding mantle. CMB regions outside of and away from LLSVPs may completely lack any notable ULVZ structure.

2. Data Sets

[8] On 15 October 2006, a relatively large earthquake (moment magnitude, $M_w \sim 6.7$) occurred near the main island of Hawaii at a depth of 38 km according to the USGS National Earthquake Information Center (NEIC) location. This earthquake was accompanied by several aftershocks; the largest aftershock, with a magnitude $M_w = 6.0$, occurred around 7 min after the main shock at a depth of 18 km (NEIC). These earthquakes are located in a distance range of 30° to 50° from stations deployed in western North America. In this distance range, *PcP* and *ScP* are predicted to have favorable reflection coefficients off the CMB for studying the deep mantle, and both phases are often observed in this distance range [*Reasoner and Revenaugh*, 2000; *Rost et al.*, 2006; *Idehara et al.*, 2007]. While Hawaiian earthquakes with magnitudes >6.0 are not necessarily uncommon, this was the first event since an $M_w = 6.2$ earthquake of 1989 (26 June). Since that time, the number of North American seismic recorders has increased dramatically. Thus we are afforded an opportunity to study the CMB in a new area with high-quality recordings. We collected data from a variety of networks, including the Northern California Earthquake Data Center (NCEDC), the Southern California Earthquake Center (SCSN), the Pacific Northwest Seismic Network (PNSN), and the Alaska Earthquake Information Center (AEIC). We also collected data from stations of USArray as part of the EarthScope initiative, the Canadian National Seismic Network (CNSN), and the Japanese Hi-Net network.

In total, roughly 1100 stations from these networks recorded the two earthquakes.

[9] The records of the main shock and the major aftershock (15 October 2006, 1707, and 15 October 2006, 1714, respectively) were investigated for the presence of *PcP* and *ScP* arrivals. No *ScP* energy was detected in the raw traces of either event likely due to the strong *S* wave attenuation in the upper mantle. Furthermore, the main shock contained no *PcP* energy at the stations analyzed. Owing to the close timing of the main shock and the aftershock, the early arriving body waves of the aftershock (such as *P* and *PcP*) have travel times that are similar to the surface waves of the main shock. However, the surface waves exhibit a dominant period that is much longer than that present for *P* and *PcP* and hence can successfully be filtered out through a narrow band pass from 0.7 Hz to 2 Hz. The filtered data reveal clear *PcP* energy above the noise level on the vertical components of many stations. The published CMT solutions of the two earthquakes are very different but the moment tensors for main and early after-shock predict good *PcP* radiation. Thus, the reason for the absence of the lack of *PcP* in the main shock remains unclear. We can therefore use the large aftershock of the Hawaiian event to study the CMB between Hawaii and the North American continent (Figure 1a).

[10] Additionally, we searched for *PcP* and *ScP* detections from the Hi-Net array in Japan, as well as from Canadian networks. Only very few traces contained *PcP* core-reflected energy above the background noise levels for CNSN (distance range from 38.5° to 39.5°), and no *PcP* (or *ScP*) evidence for Hi-Net (Figure S1 in the auxiliary material).[1] Owing to the few, if any, stations from these networks recording *PcP* and no *ScP* arrivals in either network, we did not analyze these data further.

[11] Initially, we manually selected traces that show *PcP* above the noise level in the raw data in a ±10 s time window around the theoretical *PcP* arrival time. Most of the stations did not show *PcP* energy sufficiently above the noise level, resulting in a selection of 281 good stations with clearly identifiable *PcP* energy (Figure 1c). An example of the recordings at the stations of the southern California network (SCSN) is shown in Figure 2 (the data of the other networks are shown in Figure S2). Figure 1a shows that we sample the lower mantle in a region characterized by higher than average seismic shear wave velocities [*Ritsema and van Heijst*, 2000] with the *P* wave velocity structure shown in Figure S3. An important connection between the shear velocity structure of the deep mantle and *P* wave ULVZ structure is that the LLSVP margins have been hypothesized as likely zones of ULVZ presence [e.g., *Garnero et al.*, 2007; *Garnero and McNamara*, 2008].

[12] The number of usable data varies between the networks from 104 traces for SCSN to only 26 traces from PNSN (see Table 1). The reduction in number of records is mainly due to low signal-to-noise ratio (SNR) of *PcP* arrivals, owing to noise conditions at the sites or low *PcP* energy in the theoretical *PcP* time window which could be related to changes in CMB reflectivity or CMB roughness [*Rost and Revenaugh*, 2004]. In the distance range of these data we also observe interference with phases such as *PP* and *PPP* crossing over the *PcP* arrival time window (roughly between 40° and 44°). However, we only observe minor *PP* and *PPP* energy in our high-frequency filtered data compared to *PcP* (Figure 2 and Figure S2), likely due to the multiple journeys of these phases through the strongly attenuating asthenosphere. Furthermore, both *PP* and *PPP* have a very different time-distance move out (slowness) from that of core-reflected *PcP*, and thus will not constructively sum in stacks of data at the slowness of *PcP*. Therefore these crossover phases are not expected to influence the stacks of *PcP* along the *PcP* slowness greatly. Figures S2 and S4 present both distance and back azimuth profiles of the data for the different networks.

[13] The large networks show differences between the arrivals in individual traces due to differences in raypaths and structure beneath the stations. Figures 3a and 3b show *P* and *PcP*, respectively, aligned according to theoretical travel time predictions of the 1-D Earth model IASP91 [*Kennett and Engdahl*, 1991]. Owing to local velocity variations beneath the stations and topographical differences within this large network (SCSN), the arrivals are not particularly well aligned. This is a common problem with large networks. Here we use an adaptive stacking algorithm [*Rawlinson and Kennett*, 2004] to achieve a better alignment of the *P* and *PcP* waveforms for stacking data from large networks. The individual traces are aligned using ray-theoretical travel times for a reference phase (here *P* and *PcP*) through a 1-D Earth model (model IASP91 of *Kennett and Engdahl* [1991]).

[14] A ±4 s time window is selected around the ray theoretical arrival time and linear and quadratic stacks are formed from the filtered data for these initially aligned traces, with the linear stack representing an estimate of the waveform and the quadratic stack giving an estimate of the spread of alignment between stations [*Rawlinson and Kennett*, 2004]. For each move-out corrected trace, the optimum match with the stacked trace is determined by using a direct search over time shifts τ to minimize an L_3 measure of misfit. The time shifts τ_i for the individual traces, together with the initial alignment time shifts from IASP91, are applied to each trace to improve alignment. The linear and quadratic stacks are recalculated with the improved alignments and the alignment procedure is repeated for each trace. The process is then iterated until an accurate and stable alignment for the traces is achieved [*Rawlinson and Kennett*, 2004]. This process objectively yields a stable estimate of the mean *P* and *PcP* pulse shapes, as well as a travel time residual (the shift time) for the *P* and *PcP* arrivals at each station. Many of the travel time shifts necessary for best alignment are much less than 1 s with some as big as 3 s or more (Figure S5). No *P* wave radiation nodal lines for this event are predicted to be close to the *PcP* piercing points of the lower focal sphere for the published double-couple solution. Therefore the polarities of *PcP* were not corrected. The improved alignment from adaptive stacking for *P* and *PcP* is readily apparent (e.g., see Figures 3c and 3d, respectively) and enables us to form beam traces for the direct *P* and core-reflected *PcP* arrivals.

[15] Figure 4 shows a comparison of *P* and *PcP* summation waveforms (beams) computed for data from different seismic networks. In general, instrument responses may

[1] Auxiliary materials are available in the HTML. doi:10.1029/2009JB006420.

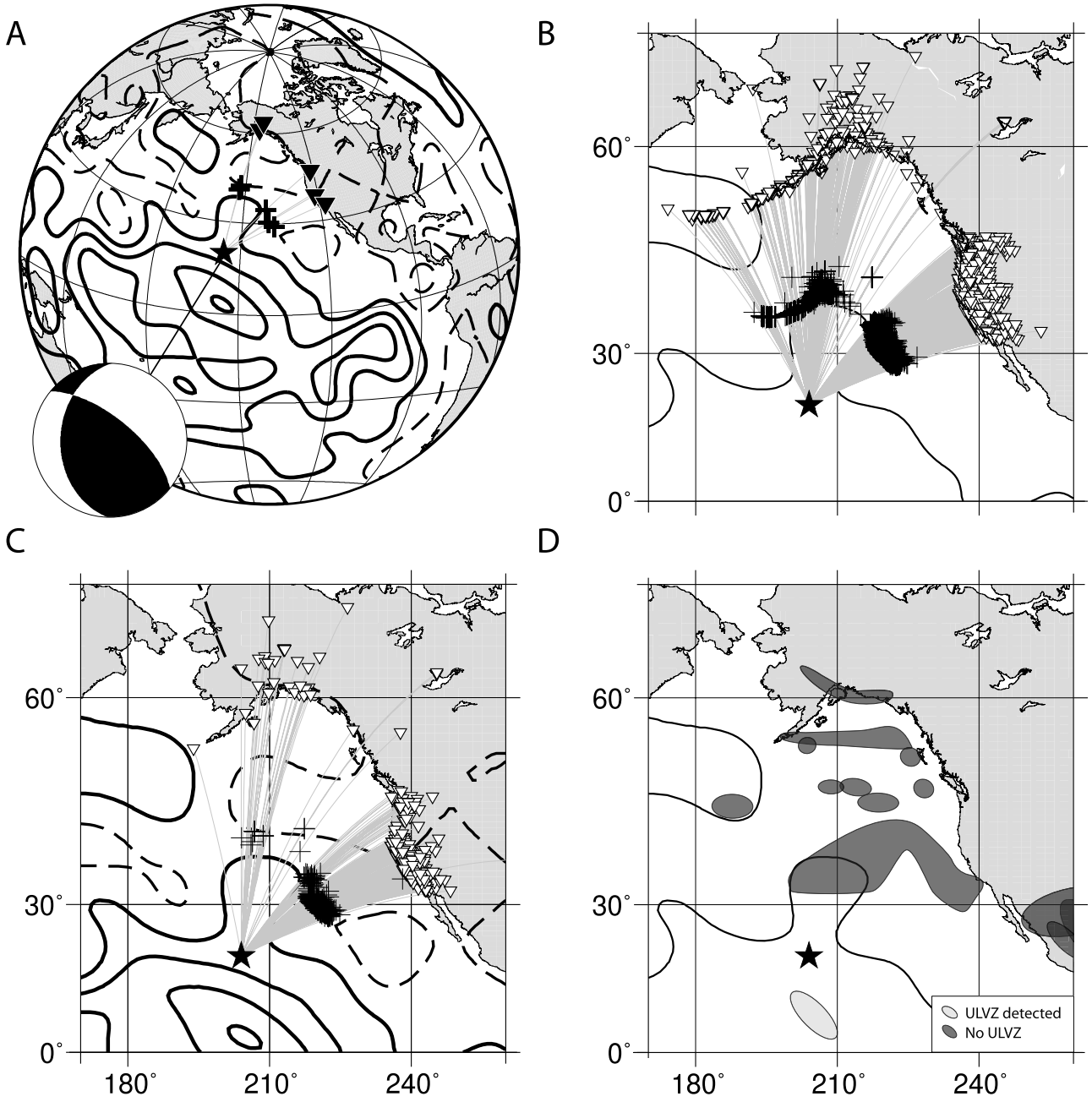

Figure 1. (a) Source-receiver path corridors from the Hawaiian earthquake (open star) to the geometric centers of western North-American networks used in this study (inverted black-filled triangles). *PcP* CMB reflection point regions are shown as crosses. Contours give tomographic velocity changes for the *S* wave model by *Ritsema and van Heijst* [2002]. Solid lines are lower than average velocities, in 0.75% intervals. The 0% contour for reduced velocity is thicker, to represent the possible boundary of the large-low shear velocity province (LLSVP) in the Pacific. The higher than average velocity contours are shown as dashed contour lines (with same interval as low velocities). The double couple solution of the earthquake (from the Global CMT Project at http://www.globalcmt.org) is shown in the insert. (b) Source (star) and receiver (triangles) combinations of all 1152 stations used in this study recording the Hawaiian earthquake. Great circle paths are shown as gray lines. *PcP* reflection points are marked by crosses. The contours are as in Figure 1a. (c) As in Figure 1b, except for stations with *PcP* adequately above the background noise level, and only the LLSVP contour is shown (and shaded). (d) Map of areas previously probed for ULVZ structure. Dark shaded areas do not show evidence for ULVZ structure while lightly colored areas show waveforms in agreement with ULVZ structure at the CMB.

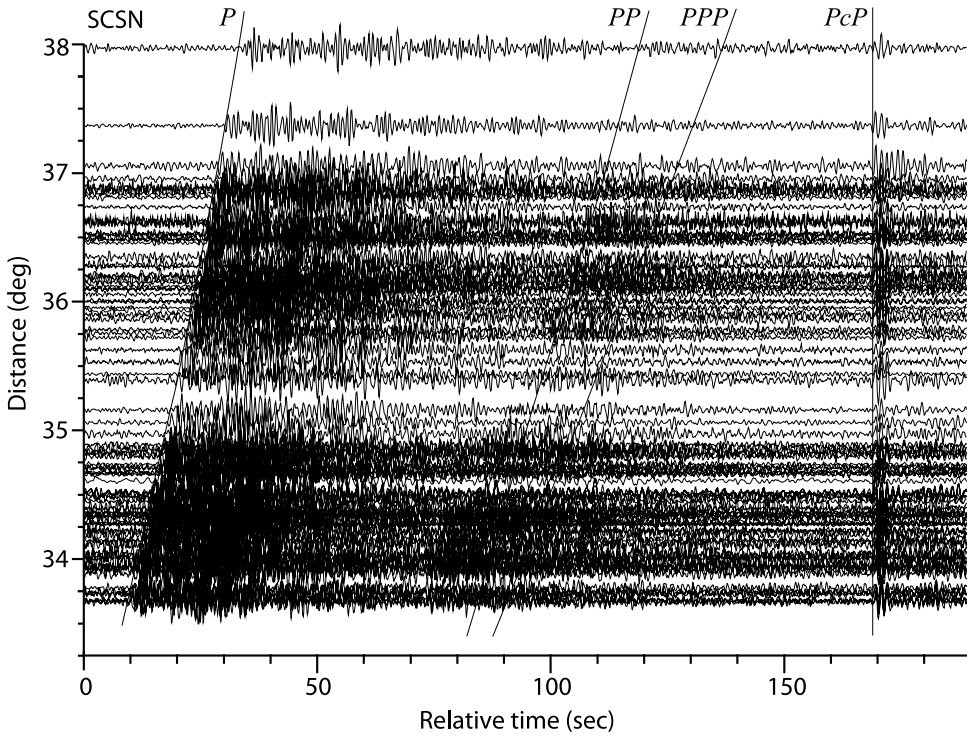

Figure 2. Data example from the Southern California Seismic Network (SCSN). Shown is ground velocity for traces selected for visible *PcP* arrivals and amplitudes have been normalized to the maximum amplitude within the time window. Traces are sorted by epicentral distance. Arrival times for *P*, *PP*, *PPP*, and *PcP* are marked. Data have been bandpass filtered with corner frequencies of 0.7Hz and 2 Hz to extract the body wave arrivals from the surface wave train of an earlier event. Data have been aligned on the theoretical *PcP* arrival for IASP91 [*Kennett and Engdahl*, 1991].

differ between seismic networks, as well as within networks. Here, we use a narrow band pass filter centered near 1 Hz to extract the *PcP* and *P* arrivals from the longer period surface wave train of the main Hawaiian earthquake. At these relatively high frequencies, *P* and *PcP* waveforms of stations within a network are sufficiently similar (e.g., see Figure 3c). Remaining waveform variations can be attributed to heterogeneity either beneath the station or somewhere else along the path. In this study we seek to find precursory arrivals to *PcP*, and thus an instrument response deconvolution is not necessary, especially given the similarity of waveforms in the 1 Hz filtered data. Nonetheless, we separately process data from different networks, as they potentially contain different waveform behavior from differently sampled CMB regions.

[16] *P* and *PcP* in the summation traces (Figure 4) display a high SNR, although sparser networks (e.g., ALBH and ALSH) have considerable noise before *PcP* compared to direct *P*. The SNR for the summation traces from the networks for *PcP* ranges from 4 to 23 (utilizing the maximum peak-to-peak amplitude in a ±10 s time window around the *PcP* arrival, divided by the maximum peak-to-peak amplitude in a 20 s time window from 40 s to 20 s before the *PcP* arrival). We choose a noise window 20 s prior to *PcP* to avoid contamination of the noise amplitude measurement with *PuP* arrivals. The SNR for *P* ranges from 3 to 22 measured similarly.

[17] No clear precursors to *PcP* can be identified above the background noise in the *PcP* beam traces of Figure 4. The waveforms of *P* and *PcP* (Figure 4) compare reasonably well; in general the *P* wavelet seems to be more complicated than *PcP*. This difference could be due to either (1) *P* and *PcP* possess slowness differences of ~ 5 s/deg and therefore have different take-off angles. The shallower take-off angle of direct *P* results in more time in the upper mantle beneath the source and receiver and thus could be prone to scattering due to enhanced heterogeneities in the upper mantle. Or, (2) with the longer path of *PcP* and its sampling of the thermal boundary layer at the base of the mantle, it may have its higher frequencies more strongly attenuated than for direct *P*. Slight broadening of the *PcP* beam relative to that of *P* is apparent, consistent with increased attenuation in the low-

Table 1. Networks and Network Codes Used in This Study[a]

Network	Code	Number of Stations	Number of PcP
Alaska Earthquake Information Center	AEIC	149	53
Pacific Northwest Seismic Network	PNSN	142	26
Southern California Earthquake Data Center	SCSN	183	104
Northern California Earthquake Data Center	NCEDC	573	94
U.S. Array	USAR	184	32

[a]Also shown is the number of stations used in the stacks.

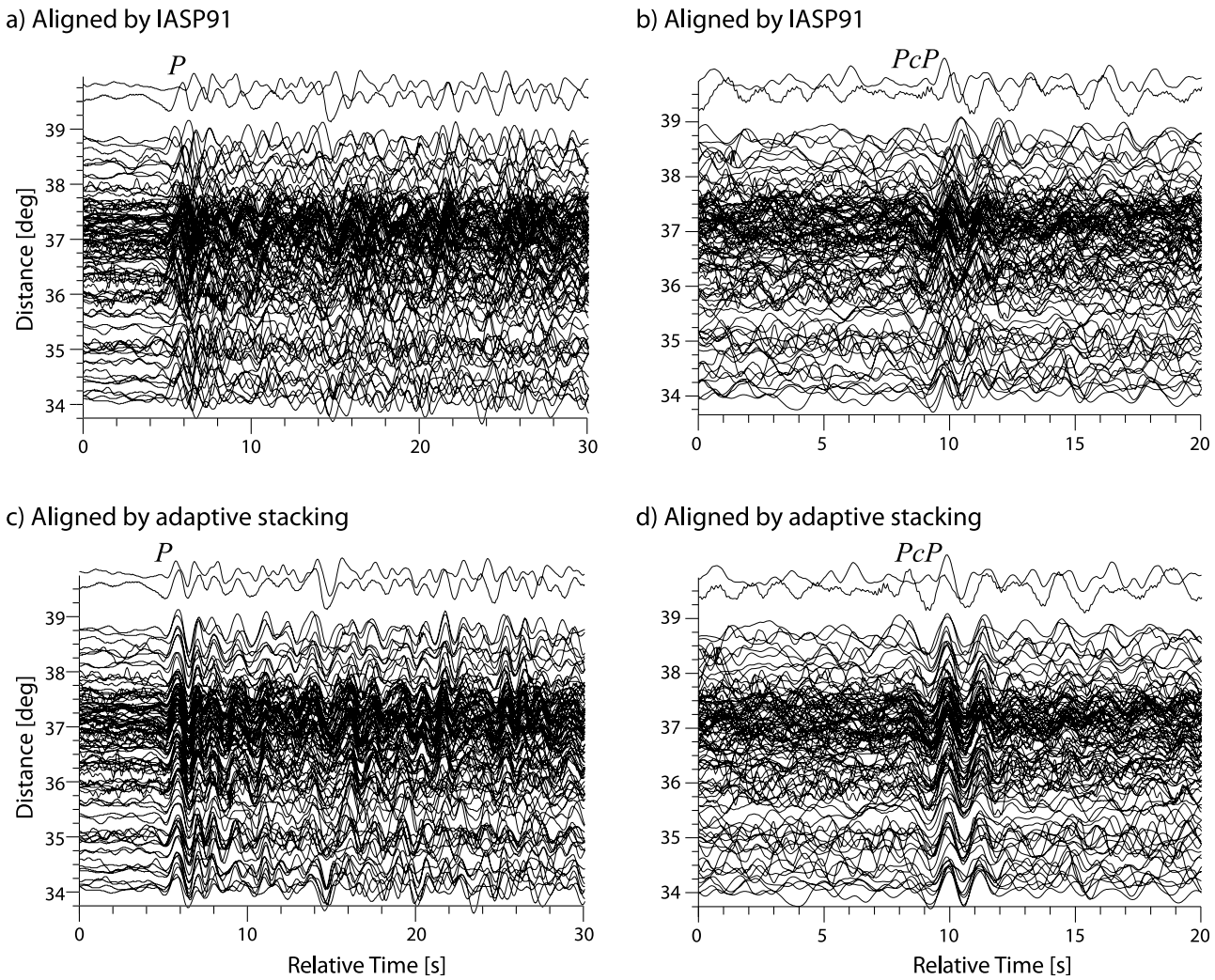

Figure 3. SCSN data showing velocity seismograms for the Hawaiian earthquake. (a) *P* waveforms aligned using theoretical travel time predictions from IASP91 [*Kennett and Engdahl*, 1991]. Velocity variations anywhere along the path, as well as topography near the receiver may be responsible for the strong observed travel time deviations. (b) As in Figure 3a but for *PcP*. (c) *P* waveform alignment after applying the adaptive stacking technique (see text for more detail), which optimally aligns the phase of interest. (d) As in Figure 3c but for *PcP*.

ermost mantle [*Rost et al.*, 2005]. Alternatively, constructive interference between *PcP* and a *P* wave reflection off the top of a ULVZ (denoted *PuP*), can effectively broaden *PcP* if the ULVZ is extremely thin (e.g., less than a few kilometers), due to the *PuP* arrival not advancing ahead of *PcP* as a separate arrival [*Rost et al.*, 2005]. Some waveform variation across the data set is also apparent. The data of the SCSN show the strongest difference between *P* and *PcP* with the initial up and downswing of *PcP* being considerably larger than being observed in *P*. This indeed could indicate reflected energy from a thin ULVZ within the CMB region covered by SCSN. Detailed analysis of the SCSN data indicates that this waveform variation originates from records sampling the eastern side of our study area. However, the waveform behavior is not laterally consistent, which precludes confidence in determination of any exact source location as the cause of the waveform differences. This is illustrated by USArray data, which have very similar *P* waveforms. However, the *PcP* data, which have very similar (overlapping) CMB bounce points, exhibit some waveform variability.

3. Modeling

[18] The recorded raw and stacked data do not show coherent evidence for *PuP* arrivals due to ULVZ layering. Synthetic modeling can be used to estimate resolution thresholds of the data set by finding models that would produce *PcP* precursors above the noise level of the data. Figure 5 shows synthetic waveforms for ULVZ models with differing properties. The synthetic waveforms were calculated using the generalized ray method [*Gilbert and Helmberger*, 1972; *Helmberger*, 1974] assuming a source-receiver distance of 37° (the average distance of our observations). Green's functions calculated for the *PcP* and *PuP* arrivals for ULVZ models have been differentiated and then convolved

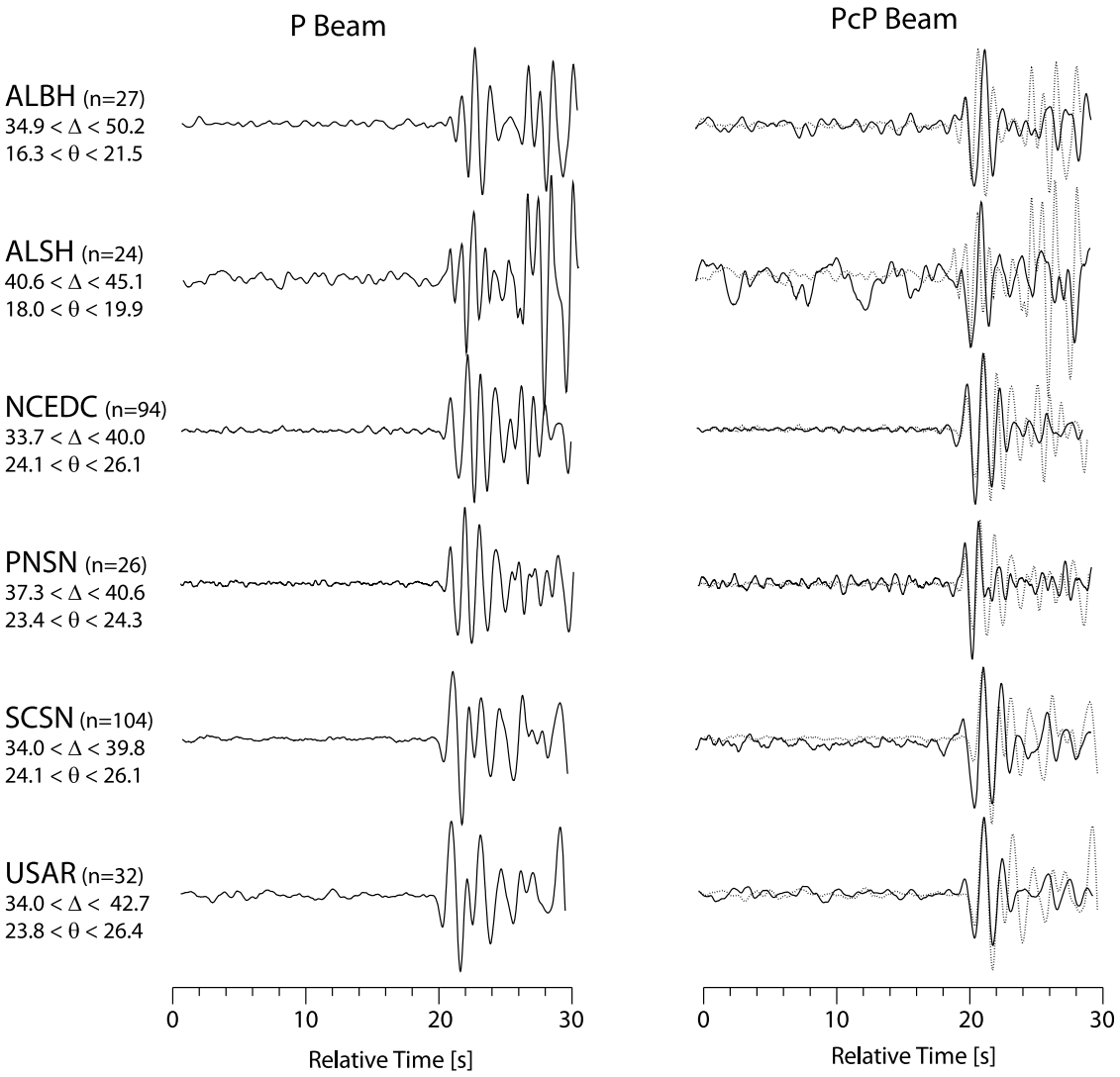

Figure 4. Beam summation traces of (left) *P* and (right) *PcP* for all networks used in this study. The *P* beam for each network is also plotted on top of the *PcP* beam, as a dashed trace. The *P* and *PcP* waveforms are in general very similar although there exist waveform variations between the networks (with USAR and SCSN being very similar in *PcP* and *P* but different than PNSN and NCEDC). The SCSN *PcP* waveform shows some deviations from *P* which could be related to very localized ULVZ structure in the sampling area, but detailed study of the individual waveforms did not reveal evidence for a compact ULVZ area. The number of records, n, in each network is indicated, along with distance (Δ) and back-azimuth (θ).

with the *P* wavelet of the stacked data from the SCSN network as the source time function (Figure 5a). These models show that the vertical resolution threshold depends on the ULVZ properties. In general, models with velocity reductions having a δV_P: δV_S ratio of 1:3 show stronger *PuP* amplitudes than models with a velocity ratio of 1:1. Strong waveform variations can be observed for thicknesses greater than 4–8 km with *PuP* amplitudes reaching more than 50% of *PcP* for some models, especially those with significant density increases (Figure 5d). A large parameter space was investigated to find possible ULVZ structures that are permissible, i.e., that produce *PuP* arrivals below our detection threshold.

[19] Figure 6 shows a summary of synthetic modeling of the *PcP* precursors. ULVZ synthetics for a range of velocity reductions have been computed to investigate the amplitude of *PuP* relative to *PcP*. We use the *PuP* to *PcP* amplitude ratio in comparison to the average noise level of the data preceding *PcP* to set constraints on ULVZ models that produce *PuP* arrivals below the data noise level and which are therefore in agreement with our observations.

[20] ULVZ models with *P* wave velocity reductions from 0 to 20% and *S* wave reductions from 0 to 50%, relative to PREM [*Dziewonski and Anderson*, 1981], were explored. Density changes with density increases relative to PREM of 0%, 5%, 10%, and 15% as well as density decreases of −5 and −9% were also investigated. The figure emphasizes combinations of ULVZ elastic parameters that result in *PuP* amplitudes above the assumed noise level of the data (small dots) or below it (larger gray circles). We use a *PcP* to *PuP*

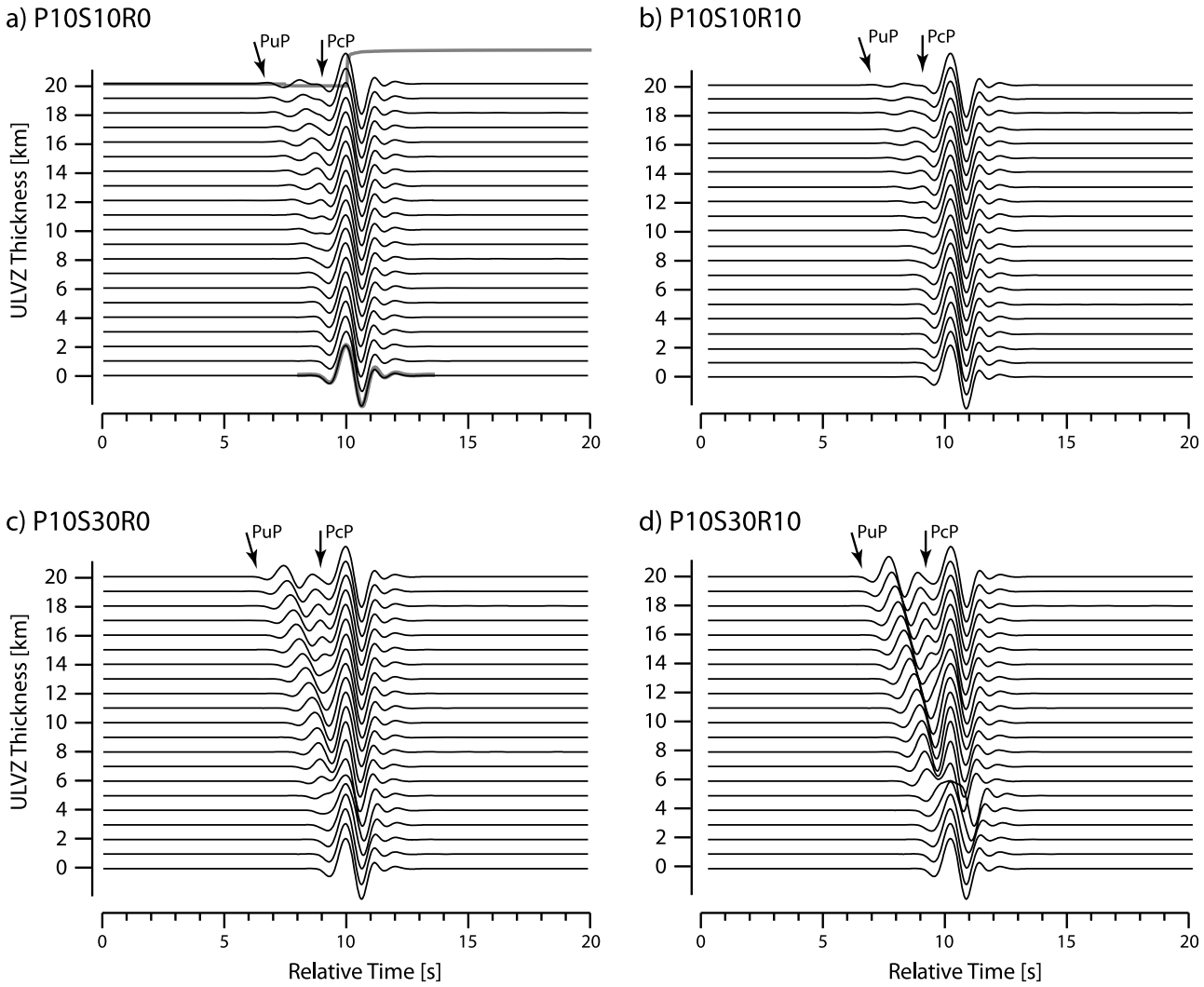

Figure 5. Synthetic waveforms for ULVZ models with thicknesses from 0 to 20 km. Synthetics have been calculated using the generalized ray method (GRM). (a) ULVZ model with 10% *P* wave (P10) and 10% *S* wave (S10) reductions and no density change (R0) compared to PREM. Top trace shows a Green's function calculated by the GRM that is used together with the source time function (from the *P* wave summation trace, shown as an underlay of the 0 km thickness trace) to produce the synthetic waveforms. Synthetics are aligned in time and amplitude on *PcP*. Energy reflected off the top of the ULVZ (*PuP*) is clearly apparent for the thicker structures. (b) As in Figure 5a but for a ULVZ model with $\delta V_P = -10\%$ $\delta V_S = -10\%$, and $\delta\rho = +10\%$ (P10S10R10). (c) As in Figure 5a but for a ULVZ model with model $\delta V_P = -10\%$, $\delta V_S = -30\%$, and $\delta\rho = 0\%$ (P10S30R0). (d) As in Figure 5a but for a ULVZ model with $\delta V_P = -10\%$, $\delta V_S = -30\%$, and $\delta\rho = +10\%$ (P10S30R10).

amplitude ratio of 8 as our detection threshold, which is the pre-*PcP* noise level for the stacked SCSN data set. Models producing *PuP* amplitudes relative to *PcP* below that threshold are marked as possible ULVZ models for our data set (i.e., showing a *PuP* nondetection).

[21] Synthetic seismograms have been calculated for a ULVZ thickness of 15 km thickness to ensure an adequate time separation of *PuP* and *PcP* for confident amplitude ratio measurements, and an epicentral distance of 37° representing an average distance of the data set. Nonetheless, we expect insignificant variations of the *PuP/PcP* amplitude ratios for other distances in the compact distance range studied here. Figure 6 emphasizes that the three free parameters result in a variety of combinations that can result in either ULVZ detection or nondetection. For absent or weak density increases in the ULVZ (i.e., 0% and 5% increase, respectively) models with $\delta V_P/\delta V_S$ of 1:1 produce *PuP* amplitudes below the noise level up to velocity reductions of ~12%, whereas most models with $\delta V_P/\delta V_S$ of 1:3 result in *PuP* above the noise level.

[22] Models with strong density increases (+10 and +15%) create *PuP* amplitudes above the noise level even for velocity ratios for $\delta V_P/\delta V_S$ of 1:1 with models with $\delta V_P/\delta V_S$ of 1:3 producing observable precursors even for weak

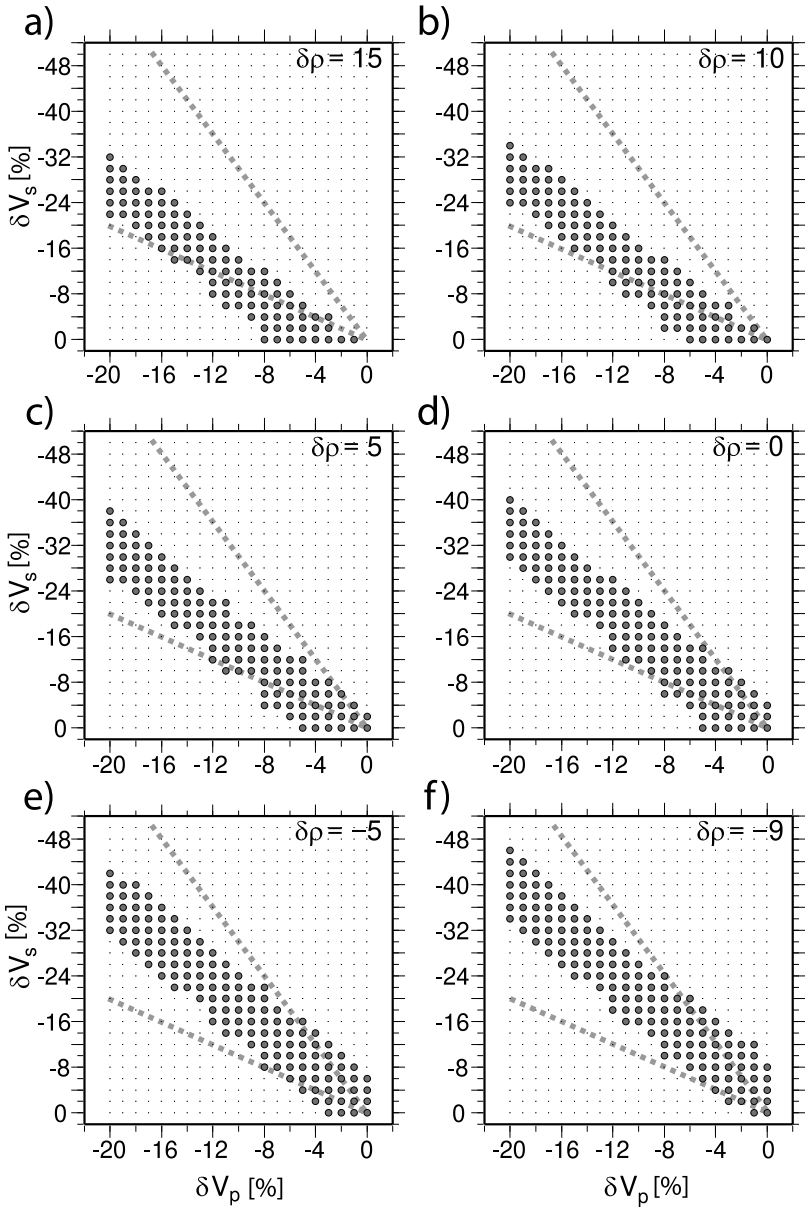

Figure 6. *PuP* detectability tests. Synthetic *PcP* and *PuP* waveforms have been calculated with GRM, and the *PuP* amplitude has been compared to the SNR of the SCSN network. Models that produce synthetic *PuP* amplitudes below the noise level of the data are indicated by gray circles. These models are in agreement with our observations. Models producing *PuP* amplitudes above the noise level in the data are indicated by small dots. The parameter space explored with these models ranges from $\delta V_P = 0$ to −20%, $\delta V_S = 0$ to −50%, and six specific density perturbations were computed (+15%, +10%, +5%, 0%, −5%, and −9%). Synthetics for this test assumed a 15 km thick ULVZ, which produces a *PuP* phase well in front of *PcP* for clear *PuP* detection. Dashed lines indicate the slope of curves that correspond to $\delta V_P/\delta V_S$ of 1:1 and 1:3. (a) A 15% density increase, (b) 10% density increase, (c) 5% density increase, (d) 0% density increase, (e) 5% density decrease, and (f) 9% density decrease.

P wave velocity reductions. For density decreases within the ULVZ, the $\delta V_P/\delta V_S$ of 1:3 models do show *PuP* amplitudes below the data noise level up to a *P* wave velocity reduction of about 8% or less. A clear differentiation of a possible density increase versus decrease within the ULVZ in the studied region is not possible from these ULVZ nondetections since either can produce *PuP* below the noise level for a wide variety of velocity reductions that can be explained physically.

4. Discussion and Conclusions

[23] The data from this Hawaiian event permit study of the lowermost mantle beneath the north-northeast Pacific using core-reflected phases. In this paper, we select the

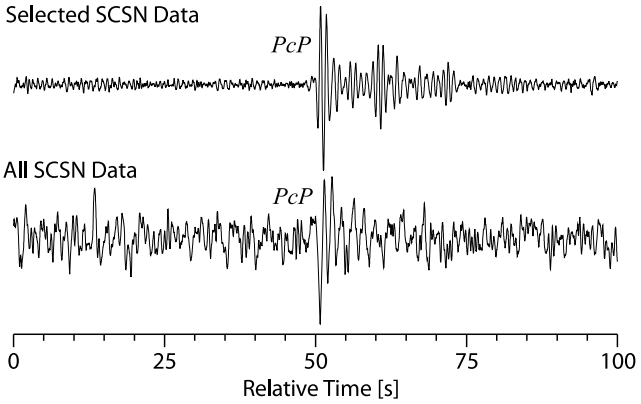

Figure 7. Comparison of *PcP* (top) in the stack of the SCSN data using the selected traces aligned using adaptive stacking techniques with (bottom) a stack using all SCSN stations aligned according to theoretical *PcP* travel times for IASP91 without adaptive stacking. Owing to the travel time differences between the stations of this large network, the *PcP* arrivals do not stack coherently and the SNR of the stacked trace is inferior to the data set of selected traces exhibiting clear *PcP*.

highest quality data for the adaptive stacking approach, which possibly could introduce a bias toward stronger *PcP* reflections. Since ULVZ structure likely reduces *PcP* amplitudes due to a reduction of the impedance contrast at the CMB, this could potentially reduce our ability to detect ULVZs in the study area when we reject low amplitude *PcP* waveforms. With the large number of data available from massive networks, it is worthwhile considering including all data in a stacking approach. Since *PcP* is not visible in all data, adaptive stacking is not possible, and we must, instead, assume a *PcP* arrival time for stacking, most likely from the prediction of 1-D Earth models. Figure 7 compares our adaptive stack of high quality data (Figure 7a, a total of 105 stacked traces) compared to stacking all data (179 traces) aligned to the *PcP* time of model IASP91 (Figure 7b). The noise level is quite high in the latter stack, due to *PcP* not being coherently summed, since *PcP* time variability is present (as noted earlier). A search for subtle precursors is therefore obfuscated with this latter approach. However, despite the high SNR in the stacked data, we observe no *PcP* precursors that are predicted by ULVZ models.

[24] To generate the network beam traces shown in Figure 4, we stacked all selected traces of each network to obtain a large signal-to-noise ratio of the *PcP* arrival. The footprints of the networks at the CMB are rather large due to the large aperture of the distributed networks and therefore we might degrade the potential signal from small-scale ULVZ structure within these footprints. Subdividing the data into smaller patches might resolve this problem and indeed we observe some waveform variation of the *PcP* arrivals with respect to their CMB reflection points. Unfortunately, the number of stacked traces in each patch becomes small enough to degrade the stability of each smaller bin stack (as evidenced from greater noise levels) and hence are not pursued here. Therefore the waveform variations remain inconclusive regarding possible ULVZ or CMB structure. Nonetheless, we note that the sampled area of the CMB might contain small ULVZ patches that are not resolved in the large scale stacking approach chosen here.

[25] Other possible explanations for our observations are (1) a ULVZ does not exist in the area sampled by our data or (2) a ULVZ is present but is too thin (<~8 km) to generate a *PuP* precursor far enough in advance of *PcP* to be separately distinguished from *PcP*. The synthetic seismograms in Figure 5 and the parameter range in Figure 6 show that even for strong velocity reductions, such as −10% and −30% in *P* and *S* wave velocities, respectively, that the ULVZ has to be thicker than ~ 5 km to produce a detectable waveform effect. Higher-frequency data potentially can resolve thinner ULVZs due to sharper waveforms [*Rost et al.*, 2006], but this data set does not contain coherent *PcP* energy above the bandpass cutoff used. The synthetics show that *PcP* is sensitive to *S* wave velocity reductions and therefore can be used to determine the ratio of *P* wave and *S* wave velocity reductions, which can be indicative of the origin of ULVZ [*Williams and Garnero*, 1996; *Berryman*, 2000; *Karato and Karki*, 2001; *Hier-Majumder*, 2008].

[26] The synthetic tests shown in Figures 5 and 6 demonstrate that a wide range of δV_P, δV_S, and ρ values result in a precursor field that would be undetectable with our data and approach. While we cannot constrain parameters of undetectably thin layering, it is fruitful to consider this possibility in relationship to previously reported deep mantle structures in this general region. Our CMB sampling region is to the north of, but near, the LLSVP beneath the Pacific Ocean (Figure 1). The LLSVPs are prominent in most global tomographic models [*Becker and Boschi*, 2002; *Garnero et al.*, 2007]. Previous studies suggest that ULVZ areas may be preferentially located near LLSVP margins [*Williams et al.*, 1998; *Garnero and McNamara*, 2008]. The boundary between LLSVPs and surrounding mantle has been seismically imaged as being a sharp transition [*Wen*, 2001; *Ni et al.*, 2002; *To et al.*, 2005; *Ford et al.*, 2006; *Wang and Wen*, 2007], supporting a chemical rather than solely a thermal origin of the low velocities. This hypothesis is consistent with the strongest lateral shear velocity gradients in tomographic models being at LLSVP edges [*Thorne et al.*, 2004]. A number of studies have now noted a geographical correlation between proposed plume activity and LLSVP margins [*Williams et al.*, 1998; *Thorne et al.*, 2004; *Torsvik et al.*, 2006], as well as a connection between ULVZ structure and deep seated mantle plume roots [*Williams et al.*, 1998; *Rost et al.*, 2005; *Garnero et al.*, 2007].

[27] Geodynamical models for thermochemical convection show that the LLSVPs can be explained by the existence of long-lived dense thermochemical piles (DTCP) located in the lower mantle [*McNamara and Zhong*, 2005], which also show increased temperatures relative to the ambient mantle. The hottest regions of the DTCP (and hence Earth's mantle) can be found at the boundaries of the chemical pile, where heat is most effectively extracted from the pile by adjacent mantle upwelling currents [*Garnero and McNamara*, 2008]. These temperature anomalies could well explain the existence of partial melt in these areas and hence is a more likely location for ULVZ presence. Convection within the DTCP can also help to stabilize dense ULVZ material toward LLSVP margins [*McNamara et al.*, 2008]; these studies demonstrate how dense ULVZ material is

predominantly stable at the CMB against DTCP margins but still active in DTCP internal convection. The contrast between ULVZ density and viscosity will determine the degree to which ULVZ material is entrained in DTCP convection and also into the mantle as DTCP material is entrained in plumes.

[28] If ULVZs are composed of dense chemically distinct material (whether or not partially molten), we expect this material to collect near pile margins. Past studies of ULVZ structure have imaged their thicknesses up to 40 km thick, with the highest-resolution methods (e.g., reflected wave studies using *PcP, ScP,* or *ScS*) predominantly assigning smaller thicknesses (e.g., 10–20 km). This thickness range is well above our detection threshold. Thus ULVZ nondetections outside of an LLSVP and away from the LLSVP margin are consistent with no ULVZ, if ULVZs are dense, chemically distinct material. Alternatively, if ULVZ is partially molten rock, whether the chemically distinct pile or the mantle is its source material, and whether or not denser than surrounding material, it may be a global feature and only detectable where thick and strong enough for seismic methods to see it.

[29] For a better understanding of the formation, evolution, and dynamics of ULVZs, an improved understanding of ULVZ distribution on Earth is necessary. This study demonstrates how even a single shallow earthquake can add to our understanding of the distribution of ULVZs, primarily due to the large seismic networks in the United States at the time of this event. While nondetections are not uncommon [*Castle and van der Hilst*, 2000; *Reasoner and Revenaugh*, 2000; *Persh et al.*, 2001; *Hutko et al.*, 2009], we emphasize the model space of this and all past studies still allows for thin, undetectable ULVZ layering. This of course permits the possibility that a ULVZ may be a global layer but thinner or weaker than what is seismically detectable in most areas.

[30] **Acknowledgments.** We would like to thank the data centers of the Northern California Seismic Network, Southern California Seismic Network, Pacific Northwest Seismic Network, Alaska Earthquake Information Center, USArray, National Research Institute for Earth Science and Disaster Prevention in Japan, and the IRIS DMC. This work was supported by CSEDI grant EAR-0456356 (SR) and NERC New Investigator grant NE/F000898/1 (SR) and grant NSF EAR-0453944 (EJG). We thank Jeroen Ritsema, Keith Koper, and an anonymous reviewer for comments that improved the manuscript. We thank Nick Rawlinson and Brian Kennett for providing the Adaptive Stacking Algorithm.

References

Akins, J., S. Luo, P. Asimow, and T. Ahrens (2004), Shock-induced melting of MgSiO3 perovskite and implications for melts in Earth's lowermost mantle, *Geophys. Res. Lett.*, *31*, L14612, doi:10.1029/2004GL020237.

Avants, M., T. Lay, and E. Garnero (2006), A new probe of ULVZ *S*-wave velocity structure: Array stacking of ScS waveforms, *Geophys. Res. Lett.*, *33*, L07314, doi:10.1029/2005GL024989.

Bataille, K., and F. Lund (1996), Strong scattering of short-period seismic waves by the core-mantle boundary and the *P*-diffracted wave, *Geophys. Res. Lett.*, *23*, 2413–2416, doi:10.1029/96GL02225.

Becker, T., and L. Boschi (2002), A comparison of tomographic and geodynamic mantle models, *Geochem. Geophys. Geosyst.*, *3*(1), 1003, doi:10.1029/2001GC000168.

Berryman, J. (2000), Seismic velocity decrement ratios for regions of partial melt in the lower mantle, *Geophys. Res. Lett.*, *27*, 421–424, doi:10.1029/1999GL008402.

Bullen, K. (1949), An Earth model based on a compressibility-pressure hypothesis, *Mon. Not. R. Astron. Soc.*, *6*, 50–59.

Castle, J., and R. van der Hilst (2000), The core-mantle boundary under the Gulf of Alaska: No ULVZ for shear waves, *Earth Planet. Sci. Lett.*, *176*, 311–321, doi:10.1016/S0012-821X(00)00027-3.

Dobson, D., and J. Brodholt (2005), Subducted banded iron formations as a source of ultralow-velocity zones at the core-mantle boundary, *Nature*, *434*, 371–374, doi:10.1038/nature03430.

Dubrovinsky, L., H. Annerstin, N. Dubrovinskaia, F. Westman, H. Harryson, O. Fabrichnaya, and S. Carlson (2001), Chemical interaction of Fe and Al2O3 as a source of heterogeneity at the Earth's core-mantle boundary, *Nature*, *412*, 527–529, doi:10.1038/35087559.

Duffy, T. (2008), Some recent advances in understanding the mineralogy of Earth's deep mantle, *Phil. Trans. R. Soc. London*, *366*, 4273–4293, doi:10.1098/rsta.2008.0172.

Dziewonski, A., and D. Anderson (1981), Preliminary reference Earth model, *Phys. Earth Planet. Inter.*, *25*, 297–356, doi:10.1016/0031-9201(81)90046-7.

Ford, S., E. Garnero, and A. McNamara (2006), A strong lateral shear velocity gradient and anisotropy heterogeneity in the lowermost mantle beneath the southern Pacific, *J. Geophys. Res.*, *111*, B03306, doi:10.1029/2004JB003574.

Garnero, E. (2000), Heterogeneity of the lowermost mantle, *Annu. Rev. Earth Planet. Sci.*, *28*, 509–537, doi:10.1146/annurev.earth.28.1.509.

Garnero, E., and D. Helmberger (1995), A very slow basal layer underlying large-scale low-velocity anomalies in the lower mantle beneath the Pacific - Evidence from core phases, *Phys. Earth Planet. Inter.*, *91*, 161–176, doi:10.1016/0031-9201(95)03039-Y.

Garnero, E., and A. McNamara (2008), Structure and dynamics of Earth's lower mantle, *Science*, *320*, 626–628, doi:10.1126/science.1148028.

Garnero, E., S. Grand, and D. Helmberger (1993), Low *P* wave velocity at the base of the mantle, *Geophys. Res. Lett.*, *20*, 1843–1846, doi:10.1029/93GL02009.

Garnero, E., J. Revenaugh, Q. Williams, T. Lay, and L. Kellogg (1998), Ultralow velocity zone at the core-mantle boundary, in *Core-Mantle Boundary Region, Geodyn. Ser.*, vol. 28, edited by M. Gurnis et al., pp. 319–334, AGU, Washington D. C.

Garnero, E., A. McNamara, M. Thorne, and S. Rost (2007), Fine-scale ultra-low velocity zone layering at the core-mantle boundary and superplumes, in *Superplumes: Beyond Plate Tectonics*, edited by D. A. Yuen et al., pp. 139–157, Springer, New York.

Gilbert, F., and D. Helmberger (1972), Generalized ray theory for a layered sphere, *Geophys. J. R. Astron. Soc.*, *27*, 57–80.

Hedlin, M., and P. Shearer (2000), An analysis of large-scale variations in small-scale mantle heterogeneity using Global Seismographic Network recordings of precursors to PKP, *J. Geophys. Res.*, *105*, 13,655–13,673, doi:10.1029/2000JB900019.

Helmberger, D. (1974), Generalized ray theory for shear dislocations, *Bull. Seismol. Soc. Am.*, *64*, 45-64.

Hernlund, J., C. Thomas, and P. Tackley (2005), A doubling of the post-perovskite phase boundary and structure of the Earth's lowermost mantle, *Nature*, *434*, 882–886, doi:10.1038/nature03472.

Hier-Majumder, S. (2008), Influence of contiguity on seismic velocities of partially molten aggregates, *J. Geophys. Res.*, *113*, B12205, doi:10.1029/2008JB005662.

Hutko, A., T. Lay, and J. Revenaugh (2009), Localized double-array stacking analysis of PcP: D″ and ULVZ structure beneath the Cocos plate, *Phys. Earth Planet. Inter.*, *173*(1–2), 60–74.

Idehara, K., A. Yamada, and D. Zhao (2007), Seismological constraints on the ultralow velocity zones in the lowermost mantle from core-reflected waves, *Phys. Earth Planet. Inter.*, *165*, 25–46, doi:10.1016/j.pepi.2007.07.005.

Karato, S., and B. Karki (2001), Origin of lateral variation of seismic wave velocities and density in the deep mantle, *J. Geophys. Res.*, *106*, 21,771–21,783, doi:10.1029/2001JB000214.

Kendall, J., and P. Silver (1996), Constraints from seismic anisotropy on the nature of the lowermost mantle, *Nature*, *381*, 409–412, doi:10.1038/381409a0.

Kennett, B., and E. Engdahl (1991), Traveltimes for global earthquake location and phase identification, *Geophys. J. Int.*, *105*, 429–465, doi:10.1111/j.1365-246X.1991.tb06724.x.

Knittle, E., and R. Jeanloz (1991), Earth's core-mantle boundary - Results of experiments at high pressures and temperatures, *Science*, *251*, 1438–1443, doi:10.1126/science.251.5000.1438.

Labrosse, S., J. Hernlund, and N. Coltice (2007), A crystallizing dense magma ocean at the base of the Earth's mantle, *Nature*, *450*, 866–869, doi:10.1038/nature06355.

Lay, T., and E. Garnero (2004), Core-mantle boundary structures and processes, in *State of the Planet: Frontiers and Challenges in Geophysics*,

Geophys. Monogr. Ser., vol. 150, edited by R. S. J. Sparks and C. J. Hawkesworth, pp. 25–41, AGU, Washington, D. C.

Lay, T., and D. Helmberger (1983), A lower mantle *S*-wave triplication and the shear velocity structure of D″, *Geophys. J. R. Astron. Soc.*, *75*, 799–837.

Lay, T., Q. Williams, E. Garnero, L. Kellogg, and M. Wysession (1998), Seismic wave anisotropy in the D ″ region and its implications, in *The Core-Mantle Boundary Region*, *Geodyn. Ser.*, vol. 28, edited by M. Gurnis et al., pp. 299–318, AGU, Washington, D. C.

Lay, T., E. Garnero, and Q. William (2004), Partial melting in a thermo-chemical boundary layer at the base of the mantle, *Phys. Earth Planet. Inter.*, *146*, 441–467, doi:10.1016/j.pepi.2004.04.004.

Lay, T., J. Hernlund, E. Garnero, and M. Thorne (2006), A post-perovskite lens and D '' heat flux beneath the central Pacific, *Science*, *314*, 1272–1276.

Mao, W., H. Mao, W. Sturhahn, J. Zhao, V. Prakapenka, Y. Meng, J. Shu, Y. Fei, and R. Hemley (2006), Iron-rich post-perovskite and the origin of ultralow-velocity zones, *Science*, *312*, 564–565, doi:10.1126/science.1123442.

Masters, G., G. Laske, and F. Gilbert (2000), Large-scale Earth structure from analyses of free oscillation splitting and coupling, in *Problems in Geophysics for the New Millennium*, edited by E. Boschi et al., pp. 255–288, Editrice Compositori, Bologna, Italy.

McNamara, A., and S. Zhong (2005), Thermochemical structures beneath Africa and the Pacific Ocean, *Nature*, *437*, 1136–1139, doi:10.1038/nature04066.

McNamara, A., E. Garnero, S. Rost, and M. Thorne (2008), Dynamics of the ultra low velocity zone, *Eos Trans. AGU*, *89*(53), Fall Meet. Suppl., Abstract DI24A-04.

Mori, J., and D. Helmberger (1995), Localized boundary-layer below the mid-Pacific velocity anomaly identified from a Pcp precursor, *J. Geophys. Res.*, *100*, 20,359–20,365, doi:10.1029/95JB02243.

Murakami, M., K. Hirose, K. Kawamura, N. Sata, and Y. Ohishi (2004), Post-perovskite phase transition in MgSiO3, *Science*, *304*, 855–858, doi:10.1126/science.1095932.

Ni, S., E. Tan, M. Gurnis, and D. Helmberger (2002), Sharp sides to the African superplume, *Science*, *296*, 1850–1852, doi:10.1126/science.1070698.

Oganov, A., and S. Ono (2004), Theoretical and experimental evidence for a post-perovskite phase of MgSiO3 in Earth's D '' layer, *Nature*, *430*, 445–448, doi:10.1038/nature02701.

Persh, S., and J. Vidale (2004), Reflection properties of the core-mantle boundary from global stacks of PcP and ScP, *J. Geophys. Res.*, *109*, B04309, doi:10.1029/2003JB002768.

Persh, S., J. Vidale, and P. Earle (2001), Absence of short-period ULVZ precursors to PcP and ScP from two regions of the CMB, *Geophys. Res. Lett.*, *28*, 387–390, doi:10.1029/2000GL011607.

Rawlinson, N., and B. Kennett (2004), Rapid estimation of relative and absolute delay times across a network by adaptive stacking, *Geophys. J. Int.*, *157*, 332–340, doi:10.1111/j.1365-246X.2004.02188.x.

Reasoner, C., and J. Revenaugh (2000), ScP constraints on ultralow-velocity zone density and gradient thickness beneath the Pacific, *J. Geophys. Res.*, *105*, 28,173–28,182, doi:10.1029/2000JB900331.

Revenaugh, J., and R. Meyer (1997), Seismic evidence of partial melt within a possibly ubiquitous low-velocity layer at the base of the mantle, *Science*, *277*, 670–673, doi:10.1126/science.277.5326.670.

Ritsema, J., and H. van Heijst (2000), New seismic model of the upper mantle beneath Africa,*Geology*, *28*, 63–66, doi:10.1130/0091-7613(2000)28<63:NSMOTU>2.0.CO;2.

Ritsema, J., and H. van Heijst (2002), Constraints on the correlation of *P*- and *S*-wave velocity heterogeneity in the mantle from P, PP, PPP and PKPab traveltimes, *Geophys. J. Int.*, *149*, 482–489, doi:10.1046/j.1365-246X.2002.01631.x.

Rondenay, S., and K. Fischer (2003), Constraints on localized core-mantle boundary structure from multichannel, broadband SKS coda analysis, *J. Geophys. Res.*, *108*(B11), 2537, doi:10.1029/2003JB002518.

Rost, S., and E. Garnero (2006), Detection of an ultralow-velocity zone at the core-mantle boundary using diffracted PKKPab waves, *J. Geophys. Res.*, *111*, B07309, doi:10.1029/2005JB003850.

Rost, S., and J. Revenaugh (2001), Seismic detection of rigid zones at the top of the core, *Science*, *294*, 1911–1914, doi:10.1126/science.1065617.

Rost, S., and J. Revenaugh (2003), Small-scale ultralow-velocity zone structure imaged by ScP, *J. Geophys. Res.*, *108*(B1), 2056, doi:10.1029/2001JB001627.

Rost, S., and J. Revenaugh (2004), Small-scale changes of core-mantle boundary reflectivity studied using core reflected PcP, *Phys. Earth Planet. Inter.*, *145*, 19–36, doi:10.1016/j.pepi.2004.02.008.

Rost, S., E. Garnero, Q. Williams, and M. Manga (2005), Seismological constraints on a possible plume root at the core-mantle boundary, *Nature*, *435*, 666–669, doi:10.1038/nature03620.

Rost, S., E. Garnero, and Q. Williams (2006), Fine-scale ultralow-velocity zone structure from high-frequency seismic array data, *J. Geophys. Res.*, *111*, B09310, doi:10.1029/2005JB004088.

Song, X., and T. Ahrens (1994), Pressure-temperature range of reactions between liquid-iron in the outer core and mantle silicates, *Geophys. Res. Lett.*, *21*, 153–156, doi:10.1029/93GL03262.

Thorne, M., and E. Garnero (2004), Inferences on ultralow-velocity zone structure from a global analysis of SPdKS waves, *J. Geophys. Res.*, *109*, B08301, doi:10.1029/2004JB003010.

Thorne, M., E. Garnero, and S. Grand (2004), Geographic correlation between hot spots and deep mantle lateral shear-wave velocity gradients, *Phys. Earth Planet. Inter.*, *146*, 47–63, doi:10.1016/j.pepi.2003.09.026.

To, A., B. Romanowicz, Y. Capdeville, and N. Takeuchi (2005), 3D effects of sharp boundaries at the borders of the African and Pacific Superplumes: Observation and modeling, *Earth Planet. Sci. Lett.*, *233*, 137–153, doi:10.1016/j.epsl.2005.01.037.

Torsvik, T., M. Smethurst, K. Burke, and B. Steinberger (2006), Large igneous provinces generated from the margins of the large low-velocity provinces in the deep mantle, *Geophys. J. Int.*, *167*, 1447–1460, doi:10.1111/j.1365-246X.2006.03158.x.

Vidale, J., and M. Hedlin (1998), Evidence for partial melt at the core-mantle boundary north Tonga from the strong scattering of seismic waves, *Nature*, *391*, 682–685, doi:10.1038/35601.

Vinnik, L., B. Romanowicz, Y. LeStunff, and L. Makeya (1995), Seismic anisotropy in the D'' layer, *Geophys. Res. Lett.*, *22*, 1657–1660, doi:10.1029/95GL01327.

Wang, Y., and L. Wen (2007), Geometry and P and S velocity structure of the "African Anomaly, " *J. Geophys. Res.*, *112*, B05313, doi:10.1029/2006JB004483.

Weber, M., and J. Davis (1990), Evidence of a laterally variable lower mantle structure from *P* waves and *S*-waves, *Geophys. J. Int.*, *102*, 231–255, doi:10.1111/j.1365-246X.1990.tb00544.x.

Wen, L. (2001), Seismic evidence for a rapidly varying compositional anomaly at the base of the Earth's mantle beneath the Indian Ocean, *Earth Planet. Sci. Lett.*, *194*, 83–95, doi:10.1016/S0012-821X(01)00550-7.

Wen, L., and D. Helmberger (1998), A two-dimensional P-SV hybrid method and its application to modeling localized structures near the core-mantle boundary, *J. Geophys. Res.*, *103*, 17,901–17,918, doi:10.1029/98JB01276.

Williams, Q., and E. Garnero (1996), Seismic evidence for partial melt at the base of Earth's mantle, *Science*, *273*, 1528–1530, doi:10.1126/science.273.5281.1528.

Williams, Q., J. Revenaugh, and E. Garnero (1998), A correlation between ultra-low basal velocities in the mantle and hot spots, *Science*, *281*, 546–549, doi:10.1126/science.281.5376.546.

Wysession, M. (1996), Large-scale structure at the core-mantle boundary from diffracted waves, *Nature*, *382*, 244–248, doi:10.1038/382244a0.

Wysession, M., T. Lay, J. Revenaugh, Q. Williams, E. Garnero, R. Jeanloz, and L. Kellogg (1998), The D ″ discontinuity and its implications, in *Core-Mantle Boundary Region, Geodyn. Ser.*, vol. 28, edited by M. Gurnis et al., pp. 273–297, AGU, Washington, D. C.

Yamazaki, D., T. Yoshino, H. Ohfuji, J. Ando, and A. Yoneda (2006), Origin of seismic anisotropy in the D ″ layer inferred from shear deformation experiments on post-perovskite phase, *Earth Planet. Sci. Lett.*, *252*, 372–378.

E. J. Garnero, School of Earth and Space Exploration, Arizona State University, Tempe, AZ 85287-1404, USA.

A. R. Hutko, National Earthquake Information Center, U.S. Geological Survey, Golden, CO 80401, USA.

S. Rost, Institute of Geophysics and Tectonics, School of Earth and Environment, University of Leeds, Leeds LS29JT, UK. (s.rost@leeds.ac.uk)

M. S. Thorne, Department of Geology and Geophysics, University of Utah, Salt Lake City, UT 84112-0001, USA.